

Reliable measurements of a 3D-printed Geneva drive

Project report in TME131 Project in Applied Mechanics

Clara Dahlberg
Frida Krohn
Filip Lindström
Gustav Onbeck
Josef Storm

DEPARTMENT OF MECHANICS AND MARITIME SCIENCES

CHALMERS UNIVERSITY OF TECHNOLOGY
Gothenburg, Sweden 2022
www.chalmers.se

PROJECT REPORT 2022

Reliable measurements of a 3D-printed Geneva drive

CLARA DAHLBERG
FRIDA KROHN
FILIP LINDSTRÖM
GUSTAV ONBECK
JOSEF STORM



Department of Mechanics and Maritime Sciences
CHALMERS UNIVERSITY OF TECHNOLOGY
Gothenburg, Sweden 2022

Reliable measurements of a 3D-printed Geneva drive
CLARA DAHLBERG, FRIDA KROHN, FILIP LINDSTRÖM, GUSTAV ONBECK, JOSEF
STORM

© CLARA DAHLBERG, FRIDA KROHN, FILIP LINDSTRÖM, GUSTAV ONBECK,
JOSEF STORM, 2022.

Supervisor: Petri Piiroinen
Examiner: Håkan Johansson and Dario Maggiolo

Project report 2022
Department of Mechanics and Maritime Sciences
Chalmers University of Technology
SE-412 96 Gothenburg
Telephone +46 31 772 1000

Cover: CAD-visualisation of the design of the Geneva drive that was used in the project.

Reliable measurements of a 3D-printed Geneva drive
CLARA DAHLBERG, FRIDA KROHN, FILIP LINDSTRÖM,
GUSTAV ONBECK, JOSEF STORM
Department of Mechanics and Maritime Sciences
Chalmers University of Technology

Abstract

A Geneva drive is a geared mechanism that transfers continuous rotational motion to intermittent rotary motion. In a Geneva drive unwanted effects such as jerk and vibrations can occur. The aim of the project consists of performing measurements of the kinematics for a chosen Geneva-drive design, both physically using a smartphone camera and simulated using MSC Adams. An internally driven Geneva-drive setup was designed using the CAD software Creo and was then 3D-printed. The physical Geneva drive's angular velocity and acceleration were analysed using a video-analysing Python script implementing a detection algorithm from the OpenCV library. In Adams a digital model of the Geneva drive was implemented and modeled to mimic the physical model as closely as possible, also measuring angular velocity and acceleration. Due to the accuracy of the detection algorithm it was concluded that a lot of the fluctuations in angular acceleration for the physical model actually is due to vibrations. Comparing angular velocity graphs from mathematical analysis, physical measurements and simulations there is a clear similarity even though the physical one has irregularities. For the angular acceleration all irregularities amplifies but similarities are visible between the theoretical and simulated values.

Keywords: Geneva drive, Computer vision, 3D printing, Adams simulations, Angular velocity, Angular acceleration

Contents

| | |
|--|-------------|
| List of Figures | viii |
| 1 Introduction | 1 |
| 1.1 Background | 1 |
| 1.2 Aim | 1 |
| 1.3 Limitations | 2 |
| 1.4 Problem definition | 2 |
| 1.5 Ethical and environmental consideration | 2 |
| 2 Theory | 3 |
| 2.1 Geneva drive | 3 |
| 2.2 Kinematics of internal Geneva drive | 4 |
| 2.3 MSC Adams and friction modelling | 6 |
| 2.4 Experimental analysis using computer vision | 6 |
| 2.4.1 Fiducial markers and computer vision | 6 |
| 2.4.2 Videos in experiments | 7 |
| 3 Methods | 9 |
| 3.1 Design and construction | 9 |
| 3.2 Experiments using computer vision | 10 |
| 3.2.1 Solution procedure for experiments | 10 |
| 3.2.2 Experiment on driving disc | 11 |
| 3.2.3 Experiment on external Geneva drive | 11 |
| 3.3 Simulations in Adams | 11 |
| 4 Results | 13 |
| 4.1 Experimental measurements on model | 13 |
| 4.2 Kinematics | 16 |
| 4.3 Adams measurements | 17 |
| 5 Discussion | 19 |
| 5.1 Design improvements | 19 |
| 5.2 Comparison | 19 |
| 5.3 Videos and computer vision as a measuring tool | 20 |
| 5.4 Adams results and improvements | 23 |
| 5.5 Summary | 23 |

Contents

| | |
|---|------------|
| A Contribution report | I |
| B Comments on the learning process | III |

List of Figures

| | | |
|------|--|----|
| 2.1 | The three different variations of a Geneva drive. | 3 |
| 2.2 | Position of the discs when the pin of driving disc enters the slot in the driven disc. | 4 |
| 2.3 | Position of discs after a small rotation from the original position. | 5 |
| 2.4 | A fiducial marker of type ArUco 4x4 with ID 0. | 7 |
| 3.1 | Finished product with the driving disc in green colour and the driven disc in orange colour. | 10 |
| 4.1 | Showcasing the important points on the Geneva drive. | 13 |
| 4.2 | Angular velocity of driven disc of internal Geneva drive. | 14 |
| 4.3 | Angular acceleration for driven disc of internal Geneva drive. | 14 |
| 4.4 | Measurements for driven disc of external Geneva drive. | 15 |
| 4.5 | Fluctuations for internal Geneva drive when disc is stationary. | 16 |
| 4.6 | Internal Geneva-drive's driving-disc angular velocity. | 16 |
| 4.7 | Angular velocity ω_2 of driven disc as a function of θ_1 . The input angular velocity ω_1 is constant for the blue line and varying as a second order polynomial for the red dashed line. | 17 |
| 4.8 | Angular acceleration α_2 of driven disc as a function of θ_1 . The input angular velocity ω_1 is varying as a second order polynomial. | 17 |
| 4.9 | Angular velocity of the driving disc as a function of time. | 18 |
| 4.10 | Angular acceleration of the driven disc. | 18 |
| 5.1 | Angular velocity ω_2 of the driven disc as a function of rotation angle θ_1 for the driving disc. A comparison of the different methods. | 20 |
| 5.2 | Angular acceleration α_2 of the driven disc as a function of rotation angle θ_1 for the driving disc. A comparison of the different methods. | 20 |
| 5.3 | Time difference between successive frames. | 21 |
| 5.4 | Comparison of marker detection when disc is stationary. | 21 |

List of Figures

1

Introduction

In this chapter, the background of the project will be presented as well as the aim and limitations. The problem definition and the ethical considerations will also be stated.

1.1 Background

A Geneva drive is a geared mechanism that transfers continuous rotational motion to intermittent rotary motion. There are several different types of Geneva drives such as external-, internal- and spherical Geneva drives. A typical design for a Geneva drive is a driving disc with a pin that rotates continuously and a driven disc that only rotates step-wise.

The driven disc has a number of slots, and when the pin on the driving disc reaches into a slot the driven disc will rotate one step. On the driven disc the number of slots can vary, where an increasing number generally leads to a smaller step-wise angle of rotation [1].

The kinematics of a Geneva drive is dependent on the size of the driving disc and what type of Geneva drive it is. When the pin enters and leaves a slot discontinuities in angular acceleration is difficult to avoid. The discontinuities mainly appear when the pin enters the slot where there is an impact between the pin and the slot wall. In theory a perfect model would not show these effects but this is difficult to achieve in a real model. Discontinuities in angular acceleration implies unwanted jerk and can lead to vibrations in the system [1].

1.2 Aim

The aim of the project was to perform reliable measurements on a Geneva drive, using physical experiments and simulations. For the physical tests the project aimed to design and 3D print a Geneva drive and construct an experimental setup driven by a servomotor, and then use that setup for measurements and data analysis. The physical measurements were done on both an internal and external Geneva drive with four slots, while the software simulations were made only on the internal Geneva drive. The designed Geneva drive was also analysed in the simulation software MSC Adams, where the aim was to get an as realistic analysis as possible so that the two methods can be used to analyse and improve each other. The aspects that were

looked upon were angular velocity and angular acceleration of the driven disc. The measurements also aimed to register impacts while the pin moved in the slots.

1.3 Limitations

During this project, the measurements and analysis on the physical model were done by filming the model in action and then use a Python script to measure the angular position, velocity and acceleration as well as detecting any discontinuities. To reduce the need of special equipment, a smartphone camera was used.

Since the time of the project was limited, the group made the decision to only design, 3D print and analyse an internal Geneva drive with four slots.

1.4 Problem definition

This project performs measurements on a 3D-printed model and MSC Adams model of an internal Geneva drive with four slots, to evaluate the accuracy of the measuring technique and validity of the Adams model. By analysing plots of the angular velocity and angular acceleration determine whether or not impacts and vibrations occur.

1.5 Ethical and environmental consideration

There are no crucial ethical aspects to take into consideration. As always, it might be favourable not to waste material and financial resources. Therefore it is important to be sure that the construction will work before the 3D-printing.

Since the Geneva drive is a construction that transfers continuous rotation to intermittent rotation, it enables the electric motor to be turned on all the time. The alternative would be to start and stop the motor to achieve the same motion as the output disc gets. That could cause fatigue in the motor a lot quicker and it would have to be replaced after a shorter time, which would be a waste of resources.

2

Theory

The theory presented in this chapter is important in order to understand how the method was developed. The theory will address Geneva drives and the kinematics behind them as well as the friction modelling in Adams and the experimental analysis using computer vision.

2.1 Geneva drive

A Geneva drive contains two discs, one driving and one driven disc. The driving disc has a continuous motion and is made up of a plate with a small pin on it, whereas the driven disc consists of a plate that has three or more slots in it. The pin of the driving disc enters these slots and rotates the driven disc [2, 3]. There are three different types of Geneva drives, which are shown in Figure 2.1.

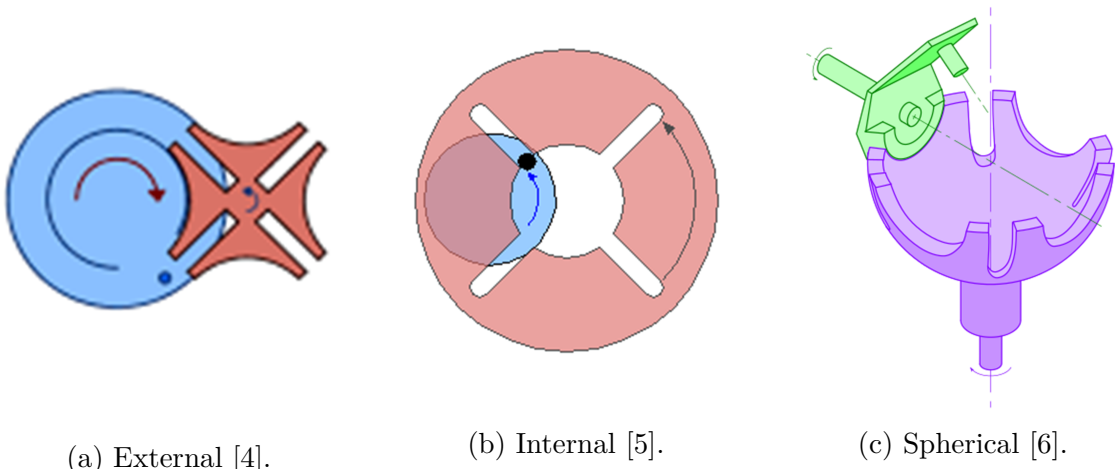


Figure 2.1: The three different variations of a Geneva drive.

The external Geneva drive, see Figure 2.1a, is the most common one and used in many mechanical products like watches and film projectors. It can be made very small and compact, and withstand high mechanical stresses [2, 3]. The angle by which the driving disc has to rotate to generate one step rotation of the driven disc is always smaller than 180° [1].

The second variant is the internal Geneva drive, see Figure 2.1b, which is larger and cannot withstand the same amount of mechanical stresses as the external one [2, 3].

The axis of the driving disc of the internal drive can have a bearing only on one side compared to the external Geneva drive that can have bearings on both sides of the disc. For an internal Geneva drive the angle by which the driving disc has to rotate to generate one step rotation of the driven disc is greater than 180° , where the switch time therefore is greater than the time the driven disc stands still [1].

For the spherical Geneva drive, see Figure 2.1c, the driving and driven disc are mounted on perpendicular shafts, which is very similar to the external Geneva drive and often used in assembly machines [2, 3].

2.2 Kinematics of internal Geneva drive

The internal Geneva drive consists of a small driving disc with a pin that pushes the rotation of a larger driven disc. The angular velocity ω_2 of the driven disc are related to the angular velocity of the driving disc ω_1 , but the relation is also dependant on the current angle θ_1 in the rotation cycle. This relation will here be derived in order to enable a comparison between the kinematics of the Geneva drive with the simulations and measurements.

Figure 2.2 shows the two discs at the moment where the pin on the small driving disc is entering one of the slots of the larger driven disc. The driving disc has its origin in point O_1 and the driven disc has its origin in point O_2 , at a distance of L . For a four-slot model, the law of sines gives

$$\frac{L}{\sin(90)} = \frac{r}{\sin(45)} \rightarrow L = \frac{r}{\sin(45)}. \quad (2.1)$$

This relation between L and r will later be used.

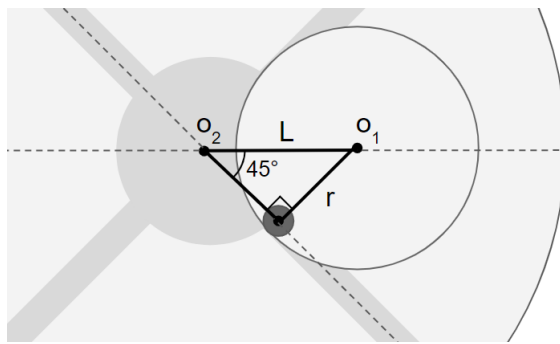


Figure 2.2: Position of the discs when the pin of driving disc enters the slot in the driven disc.

After a short time, the discs have rotated slightly and are in the position depicted in Figure 2.3. The rotational angle of the small disc, θ_1 , and the rotational angle of the large disc, θ_2 are introduced in Figure 2.3. The distance between the origins is still L and the distance to the center of the pin from O_1 is still r but the length of the third side of the triangle have changed.

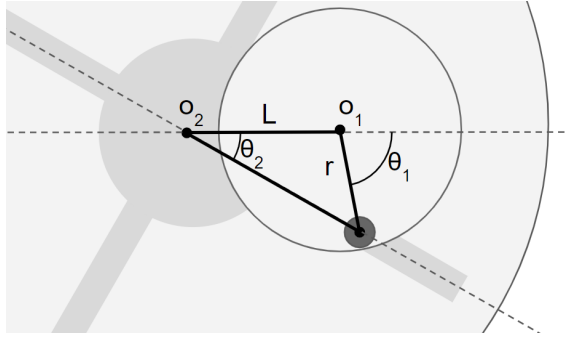


Figure 2.3: Position of discs after a small rotation from the original position.

Now, referring to the length of the third side in the triangle ℓ and solving for the vertical and horizontal components of the triangle gives

$$\ell \sin(\theta_2) = r \sin(180 - \theta_1) = r \sin(\theta_1) \rightarrow \ell = r \frac{\sin(\theta_1)}{\sin(\theta_2)} \quad (2.2)$$

and

$$\ell \cos(\theta_2) - r \cos(\theta_1) = L. \quad (2.3)$$

Inserting equation (2.2) into equation (2.3) gives

$$-\cos(\theta_1) + \frac{\sin(\theta_1)}{\tan(\theta_2)} = \frac{L}{r}. \quad (2.4)$$

Rewriting equation (2.4) using equation (2.1) gives

$$\tan(\theta_2) = \frac{\sin(\theta_1)}{\frac{L}{r} + \cos(\theta_1)} = \frac{\sin(\theta_1)}{1/\sin(45) + \cos(\theta_1)}. \quad (2.5)$$

This gives further that

$$\theta_2 = \arctan\left(\frac{\sin(\theta_1)}{1/\sin(45) + \cos(\theta_1)}\right). \quad (2.6)$$

By time differentiating equation (2.6) with respect to the angles, the following relation between the angular velocities of the two discs is obtained as

$$\omega_2 = \left(\frac{a \cos(\theta_1) + 1}{1 + a^2 + 2a \cos(\theta_1)}\right) \omega_1 \text{ with } a = 1/\sin(45), \quad (2.7)$$

where ω_1 is the angular velocity of the driving disc and ω_2 is the angular velocity of the driven disc. This is a valid relation for $\theta_1 = [-135^\circ, 135^\circ]$, which is the three quarters of a revolution when the pin is in the slot. To get a relation between the angular accelerations of the two discs, equation (2.7) has to be time differentiated again, giving

$$\alpha_2 = \left(\frac{a \cos(\theta_1) + 1}{1 + a^2 + 2a \cos(\theta_1)}\right) \alpha_1 + \left(\frac{a \sin(\theta_1)(1 - a^2)}{(1 + a^2 + 2a \cos(\theta_1))^2}\right) \omega_1^2, \quad (2.8)$$

where α_1 is the angular acceleration of the driving disc and α_2 is the angular acceleration of the driven disc. If the angular velocity of the driving disc were to be constant, the first term in equation (2.8) vanishes since α_1 in that case is zero. Equations (2.7) and (2.8) will be used for comparing the simulations and measurements to the mathematical kinematic of the model.

2.3 MSC Adams and friction modelling

MSC Adams is a dynamics and motion analysis software where mechanisms of one or several rigid bodies can be simulated on how they affect each other under added load and motion. Adams is useful to study kinematics and resultant forces caused by for example friction. It can import models created in CAD software, which is utilized in this project.

Friction will affect the Geneva drive's motion, both in the driven disc's bearing and in the contact between the two discs. There are several ways to model friction, partly depending on the desired accuracy. Since the friction on the 3D-printed model will be difficult to establish, due to the imperfections in the construction, a Coulomb friction was used for the simulation model. In a Coulomb friction model the magnitude of the kinetic friction coefficient is constant, but a change of direction will change the sign in front of the friction coefficient. The relation is given by $F_f \leq \mu F_n$ where F_f is the friction force, F_n is the normal force between the two surfaces and μ is the friction coefficient [7]. For plastic similar to the one used for 3D printing the static and kinetic friction coefficients used were $\mu_s = 0.194$ and $\mu_k = 0.089$ [8].

Over rotation of the driven disc can occur in this kind of internal Geneva drive. The over rotation is caused by imperfections such as gaps between the pin and the slots that leads to impact. The problem can be fixed by adjusting the model to eliminate the cause or counteract the resulting issue by increasing the friction in the bearing to stop the motion of the driven disc earlier.

2.4 Experimental analysis using computer vision

The following sections explain the concepts important for the experimental method and its subsequent analysis.

2.4.1 Fiducial markers and computer vision

A fiducial marker is a reference object placed in the field of view to simplify the extraction of information from an image captured of this field of view. Some fiducial makers are made with the sole purpose of being easily recognized by a computer-vision algorithm, where ArUco is one of them [9, 10]. Since computer-vision algorithms utilise contour lines where the colour value is different on either side, fiducial markers are typically made in black and white with straight lines. Figure 2.4 shows the fiducial marker used in this project.

Computer vision is the application of algorithms to detect regions in an image that define an object of predefined appearance. The computer-vision algorithm for the ArUco marker applies adaptive thresholding and a contour function as the primary image processing algorithms followed by steps to reduce the amount of possible candidates. The last step is to attempt to read the grid and deduce what ID it corresponds to within the library [11].

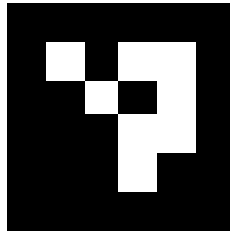


Figure 2.4: A fiducial marker of type ArUco 4x4 with ID 0.

2.4.2 Videos in experiments

When a video is made it is typical that a frame rate is defined, the rate at which images are captured and displayed, where 30 or 60 frames per second are common. When an image is captured for the purpose of being included in a video the procedure is slightly different from when an image is captured normally. The image needs to be decoded to reduce space, 30 or 60 frames per second would very rapidly deplete the storage of whatever device is used to capture and store the images on. This procedure of capturing images and instantly decoding require a lot of computing power for a fine resolution. The decoding procedure makes use of the fact that much of the information in the image remains the same between individual frames, but when this is no longer the case the time between frames might increase which leads to a varying frame rate [12].

Image resolution is the amount of pixels, square-shaped cells of equal size with a constant colour, present in an image. The colour is typically defined in the RGB scale with 3 values, each value defines how red, green, and blue the cell is from 0-100% where 100% in 8-bit is the numerical value of 255.

When the fiducial marker is to be captured in an image the concept of image space utilization is of interest. As previously mentioned, an image contains a set of pixels that discretize the projection of objects in the field of view. When measurements are to be done using the representation of the fiducial marker(s) inside the image the space they utilize is of importance. When the fiducial marker is small and image space it utilizes is maximised the margin of error for any measurements is minimized. This is a result of translating a distance inside an image from pixels to meters. When the fiducial marker is placed in the field of view the size in millimeters is known, this means when the same size is defined in pixels a function relating the two can be found.

When working with images or videos it should be noted that the pixels representing the colors of the object captured can be slightly changed due to something called image noise , which can cause a pixel in one instance to contain the RGB value [0, 0, 0] and in a next instance contain the value [10, 10, 10] for example [13].

2. Theory

3

Methods

This chapter describes the methods that were used for the different parts of the project.

3.1 Design and construction

An internal Geneva drive was chosen to be made by first creating a CAD model, which was then 3D printed and motorized.

The choice of an internal Geneva drive means that a smaller disc with constant angular velocity should drive the rotation of a bigger disc. The smaller disc therefore had to be placed inside the radius of the larger disc, either above or underneath. This created design difficulties since the shafts holding the discs together can not be mounted on both sides of the discs. They can only have rotational bearings on one side. The bearings, especially the one in the small disc, needs to take up undesired bending moment. This bending moment is created when the pin on the small disc is hitting the larger disc.

After some initial sketches, the design was created using the CAD-software Creo parametric [14]. The different parts were created separately as individual parts and then assembled into an assemble design. This made it possible to simulate the rotational motion directly in the CAD software to make sure that radiiuses and the part placements were right. Since the model was to be 3D printed, an important part of the design process was to come up with geometries that were easy to print without support material. The fixture therefore had to be split up into four different parts. To make sure that the axis and disc had a good fit to the ball bearings, small holes and pegs were 3D printed. In that way, a good fit was secured by some trial and error. A holder for the servo motor was designed on top of the fixture. To make sure that the motor would fit, a 3D model of the motor was sketched in the CAD software as well and added into the Creo assembly.

The design was then 3D printed using a 3D-printer of model Ultimaker S5 and Ultimaker S3 extended. After 3D printing, the different parts were mounted together with press fit and a total of 12 screws. The servo motor was controlled by an Arduino and a small script setting the angular velocity of the driving disc. After some initial tests, the rotational friction of the driven disc was slightly increased to minimize the risk of over rotation. The finished model is shown in Figure 3.1.

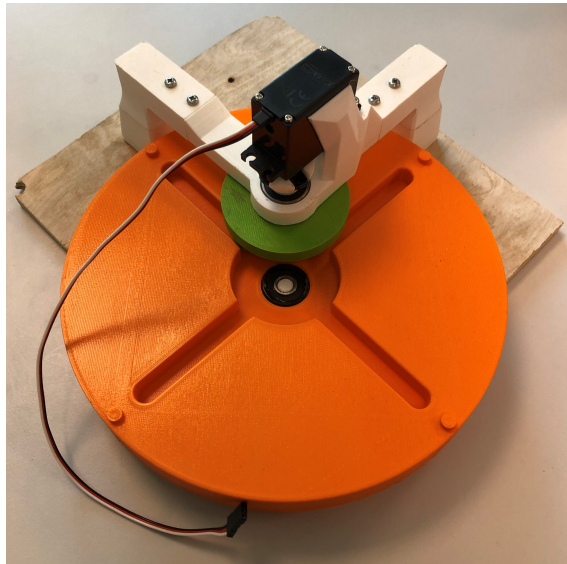


Figure 3.1: Finished product with the driving disc in green colour and the driven disc in orange colour.

3.2 Experiments using computer vision

This section explains the solution procedure of the experimental method and the experiments that were performed. The experimental method utilises videos and computer vision, section 2.4 explains information regarding this. The experiments were performed on the driven disc of both an internal and external Geneva drive as well as the driving disc of an internal Geneva drive.

3.2.1 Solution procedure for experiments

The first step was to generate videos while the discs were in motion. The model was set up such that the fiducial marker never exited the field of view, for a Huawei-p20pro camera this implied a distance between the camera and the model of roughly 30 centimeters. The resolution in the video captured on the Huawei-p20pro camera was 3840x2160, which is also known as 4K UHD.

The first step in analysing the video was to extract the presented timestamps in the metadata. The metadata was obtained using the program FFmpeg [15] and the presented timestamps could be extracted using a regular expression on the text file obtained.

In the next step the video was separated into frames. The computer-vision algorithm for the fiducial marker was utilised from the OpenCV library which gave the corners and ID's of every found fiducial marker of the given dictionary. The fiducial marker type or dictionary used for these tests were ArUco 4x4. The ID used for the driven disc was ID 0, markers found with this ID in the frame were extracted and the corners x - and y -values stored. Using the x - and y -values of the corners a center point of the marker was also obtained through averaging.

When all the frames had been analysed by the computer-vision algorithm the next step was to determine the center of rotation for the driven disc. For a given time step, five positional values were given for the disc, the four corners of the marker and the center of the marker. Any of the positional values had a constant distance to the center of rotation, for only two points the location is impossible to specify since the radius is unknown. A function that defines all center points for circles including two points is derived

$$f(x, x_1, y_1, x_2, y_2) = \frac{y_1 + y_2}{2} + \frac{x_2 - x_1}{y_2 - y_1} \frac{x_1 + x_2}{2} - \frac{x_2 - x_1}{y_2 - y_1} x, \quad (3.1)$$

where x_1 , y_1 , x_2 , and y_2 are the x and y values of the 2 points of the same type, corner 0 for example.

Using two different positional values for two different time instances, two different functions from equation (3.1) could be found. By converting the linear equations to vectors the intersection point in 2-dimensions could be found using the cross product.

By calculating the angle with respect to the center of rotation, each of the five points would represent a signal for the rotation angle of the whole disc. By assuming a constant slope in between points of the same signal an angular velocity and angular acceleration could be calculated using the time values from the video metadata.

It was of interest to evaluate whether or not the model vibrates when stationary as a result of the driving disc rotating freely.

3.2.2 Experiment on driving disc

The conversion between continuous to intermittent motion requires the motor to apply a varying torque to accomplish a constant angular velocity of the driving disc. It was therefore of interest to monitor the angular velocity of the driving disc to monitor if a constant velocity was in fact applied. Otherwise the comparison with the analytical solution and the Adams solution would be off. The angular velocity of the driving disc was measured in the same way as the driven disc using fiducial markers and a video capturing the motion.

3.2.3 Experiment on external Geneva drive

Experiments were also performed on an external Geneva drive, for comparison's sake, with rotation constraint making over-rotation impossible. The experimental method used on the external Geneva drive were the exact same as for the internal Geneva drive.

3.3 Simulations in Adams

When the model was simulated in Adams, the two rotating discs were imported from the CAD model and assembled with a distance of 25 mm between the two axes. To

3. Methods

simplify the assembly process only the discs were imported, since they were the moving parts. Because the supportive construction parts do not contribute to the kinematics, they were not included in the simulations. Revolute joints were used to constrain the discs to only allow rotation around their axis and to prohibit translational motions, resulting in one degree of freedom per disc. The contact between the pin and the path in the driven disc was defined such that the rotational motion could be transferred. The friction was assumed to follow the Coulomb friction model with a static friction coefficient of 0.194 and a dynamic friction coefficient of 0.089, according to section 2.3. The friction in the axis of the driven disc was step-wise increased to minimize over rotation. The weights of the discs were implemented to the part properties. They were known from the 3D-printed models as 17 g for the driving disc and 348 g for the driven disc. The input angular velocity, coming from the motor, was implemented as a non-constant angular velocity. This input data comes from the results, Figure 4.6 shows how the angular velocity of the driving disc varies.

When the simulation was started, only one sequence was analyzed, which was a 270°-rotation of the driving disc. Graphs describing angular velocity and angular acceleration for the driven disc were generated. The number of time steps in the simulation was increased until convergence had been reached. However, two simulations were made, one using the original dimensions of the discs and one with an increased pin diameter. The pin diameter in the original drawing was 0.5 mm smaller than the width of the slot of the driven disc. This freeplay between the parts was eliminated in the second simulation where the pin diameter was increased to 10 mm, the same width as the slot in the driven disc.

4

Results

This chapter will present the results of the analytic, simulated and physical measurements of the Geneva-drive kinematics.

4.1 Experimental measurements on model

Figure 4.1 shows a frame from the video used to evaluate the driven disc of the internal Geneva drive. Three different colored circles showcase points of interest, the light blue circles are the corners of the detected fiducial marker, the pink is the center of the fiducial marker, and the red is the center of rotation of the driven disc. The circles are generated by an OpenCV function called circle using the values from the calculations.



(a) Camera view.

(b) Zoomed view of the fiducial marker.

Figure 4.1: Showcasing the important points on the Geneva drive.

The following figures, Figure 4.2 and 4.3, showcase the angular velocity and angular acceleration for the marker's corners as well as the marker's center. The marker center is a more stable and more precise signal.

Figure 4.2 shows the angular velocity for the corners of the fiducial marker and the center of the fiducial marker for the internal Geneva-drive's driven disc. From the time 3 to 4 s the disc is stationary but shows small deviations from zero. At 4 s a sharp drop in angular velocity can be observed down to -0.6 rad/s. The local

4. Results

minimum for the sequence 4 to 7 s occur at 5.5 s with a value of -0.675 rad/s. During the drive cycle 4 to 7 s the angular velocity appears spiky and change direction constantly.

Large deviations from zero can be observed during stationary use for the marker corners, these are results of the detection algorithm misplacing the corners further into the marker.

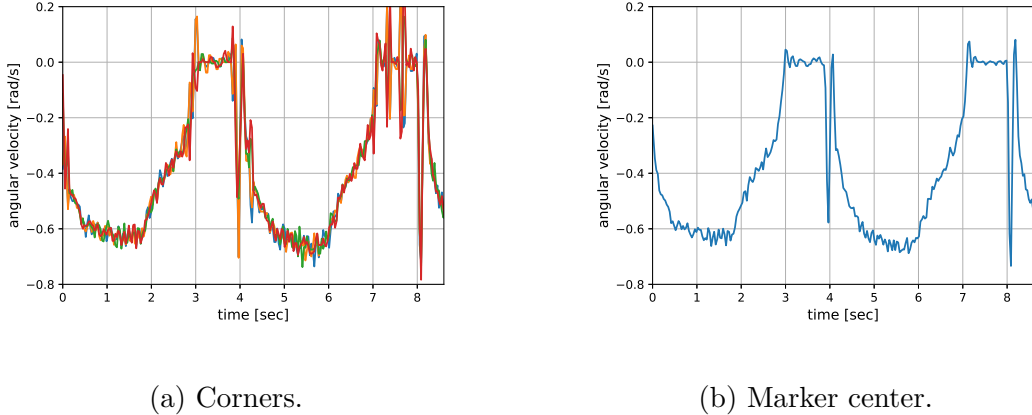


Figure 4.2: Angular velocity of driven disc of internal Geneva drive.

Figure 4.3 shows the angular acceleration for the corners of the fiducial marker and the center of the fiducial marker for the internal Geneva-drive's driven disc. At 4 and 8 s, large accelerations can be observed coinciding with the spikes in angular velocity observed in the previous figure, Figure 4.2. After the spike at 4 s, the angular acceleration appears slightly negative until 5.5 s when the local minimum of the velocity occurs. At 5.5 s the acceleration switches sign and appears slightly positive until 7 s when the disc is again stationary. The acceleration of the corner points show large spikes during the stationary sequence of 7 to 8 s.

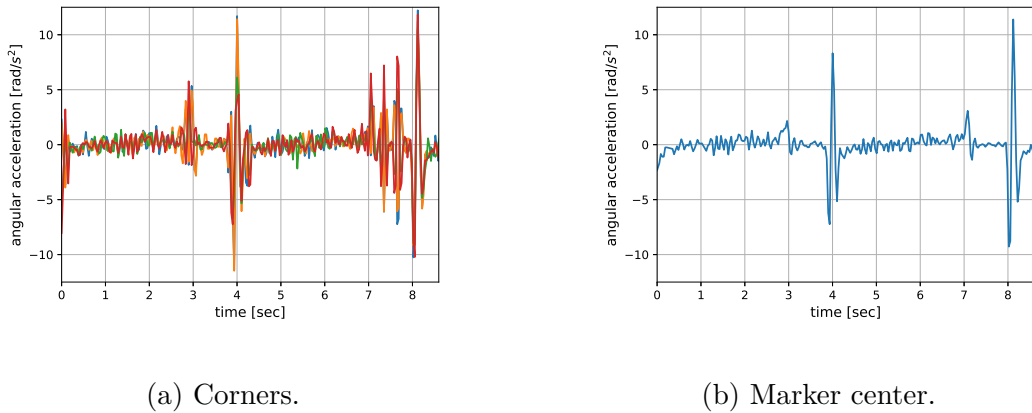
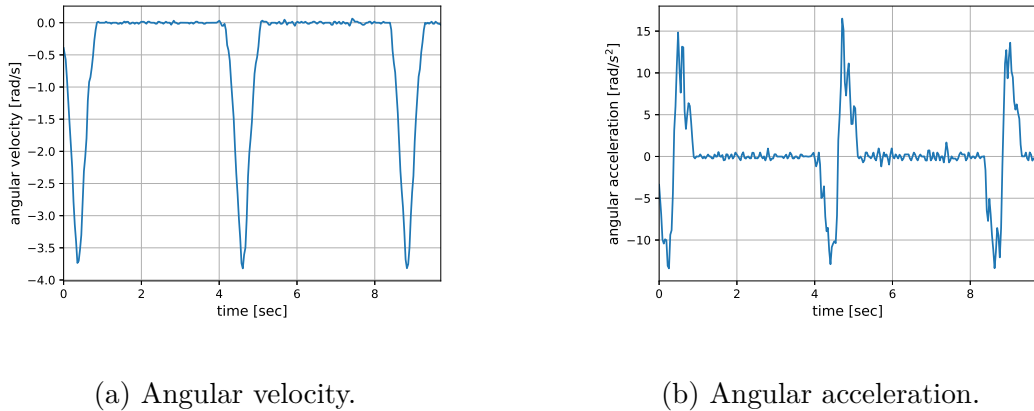


Figure 4.3: Angular acceleration for driven disc of internal Geneva drive.

Figure 4.4 shows measurements for the angular velocity and the angular acceleration for the marker center of the external Geneva drive. The external Geneva drive shows a much shorter drive sequence of 1 s and a 3 s stationary sequence. The local minimums of the drive sequences coincide well at a value of -3.75 rad/s. The angular velocity does not change direction before the local minimum. During the stationary sequence some deviations from zero can be observed for both the angular velocity and angular acceleration.

During the drive sequences the angular acceleration is strictly negative before the local minimum of the angular velocity and strictly positive after the local minimum. The largest negative value can be observed right before the change in sign at about -12 rad/s² and the largest positive right after the change at about 12 to 15 rad/s². The acceleration shows some spikes during the drive sequence.



(a) Angular velocity.

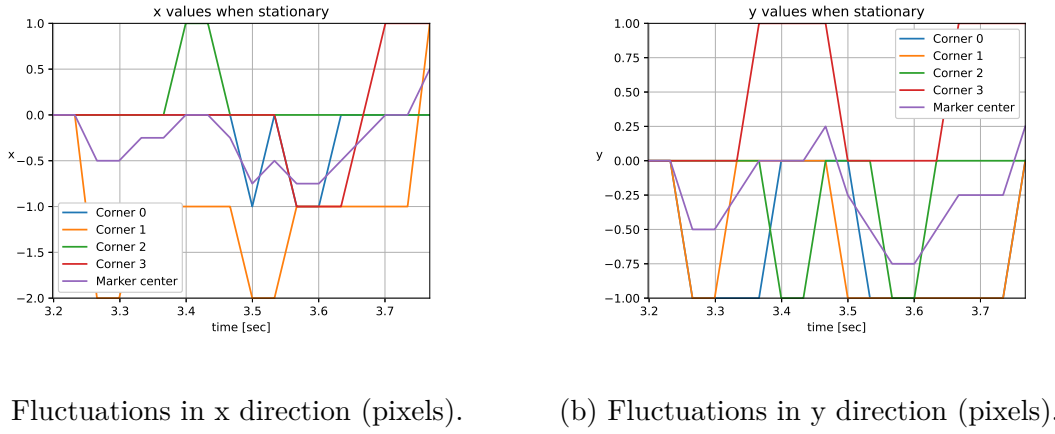
(b) Angular acceleration.

Figure 4.4: Measurements for driven disc of external Geneva drive.

Figure 4.5 shows the fluctuations of the fiducial marker corners and center during a stationary sequence for the internal Geneva-drive's driven disc. Figure 4.5 shows the *x*-fluctuations and the *y*-fluctuations. The corners and marker center were normalized at the first time instance showed of 3.2 s. The corners can only deviate a full pixel since they are directly defined by the detection algorithm but the marker center being the average *x*- and *y*-values of the corners can vary in fractions of a pixel. In Figure 4.5a the largest deviation is two pixels and in Figure 4.5b the largest deviation is one pixel. The different corners show very little correlation between deviations implying independent reasons for the deviations. The marker center never deviates more than 0.5 pixels in either *x*- or *y*-direction in a single time step. Similar results were found when evaluating the external Geneva-drive's driven disc.

In section 2.4, the connection between the pixel size of a fiducial marker and its real size is explained. By using a marker with a size of 32 by 32 mm, and 164.76 by 162.59 in pixels that implies for this test that a pixel corresponds to 0.195 mm.

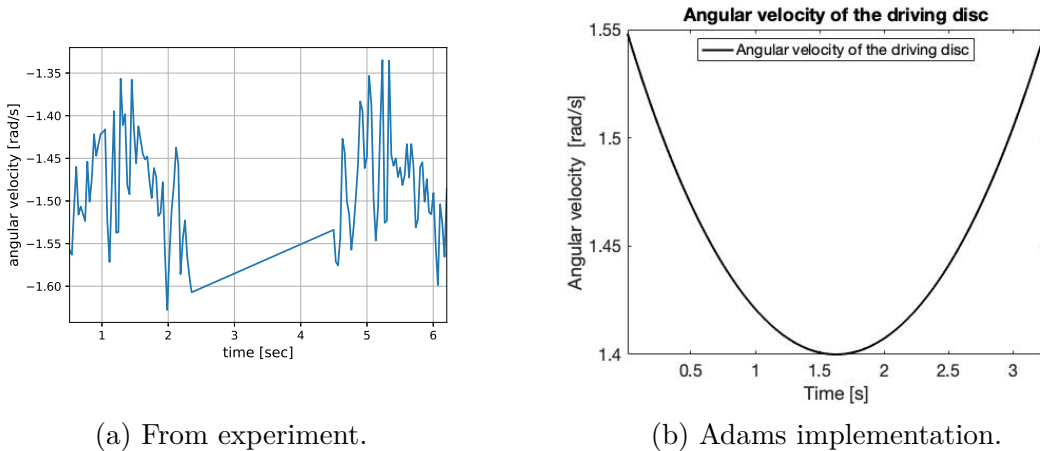
4. Results



(a) Fluctuations in x direction (pixels). (b) Fluctuations in y direction (pixels).

Figure 4.5: Fluctuations for internal Geneva drive when disc is stationary.

Figure 4.6 shows the angular velocity of the driving disc during a driving sequence for the experiments and the Adams implementation. For Figure 4.6a, at 0 and 4.5 s the driving pin has entered the slot of the driven disc, and at 2.3 and 6.2 s the driving pin is just about to exit the slot completing the driving sequence. For Figure 4.6a, from 2.3 to 4.5 s the fiducial marker is obscured by the motor and support structure. The input velocity can be modeled by assuming a mirrored behaviour during the obscured sequence when the driving pin just enters as a second order polynomial with a local maximum of -1.4 rad/s and local minimums of -1.55 rad/s at either end.



(a) From experiment.

(b) Adams implementation.

Figure 4.6: Internal Geneva-drive's driving-disc angular velocity.

4.2 Kinematics

Figure 4.7 shows the kinematic relation between the velocity of the driven disc ω_2 and the velocity of the driving disc ω_1 as a function of θ_1 . The relation is derived in section 2.2 and stated in equation (2.7). The blue solid line in the figure shows the relation when the driving velocity of the small disc is constant at 1.55 rad/s

while the red dashed line shows the relation when the input angular velocity of the driving disc is varying. In this case, the input angular velocity ω_1 is chosen to vary as a second degree polynomial, as plotted in Figure 4.6b. This is the same angular velocity that is used as the input in the Adams simulations. In a corresponding way, Figure 4.8 shows the angular acceleration α_2 as a function of θ_1 for the constant and varying case of input angular velocity ω_1 . The algebraic relation for the angular acceleration is stated in equation (2.8).

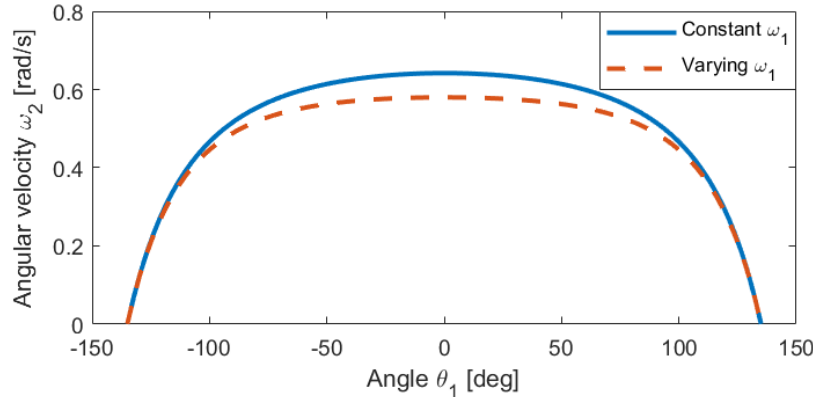


Figure 4.7: Angular velocity ω_2 of driven disc as a function of θ_1 . The input angular velocity ω_1 is constant for the blue line and varying as a second order polynomial for the red dashed line.

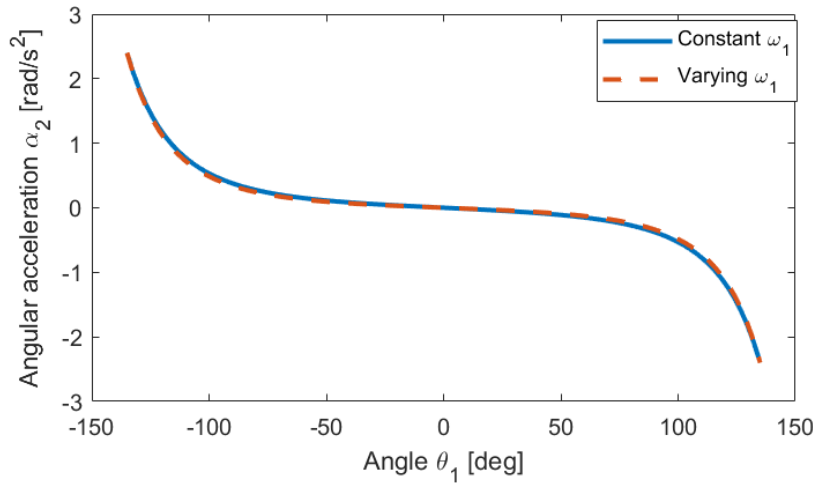


Figure 4.8: Angular acceleration α_2 of driven disc as a function of θ_1 . The input angular velocity ω_1 is varying as a second order polynomial.

4.3 Adams measurements

When the rotational motion is transferred to the driven disc, its angular velocity reaches a plateau at 0.58 rad/s which can be seen in Figure 4.9. When the pin

4. Results

diameter is increased to 10 mm and the gap is eliminated, the maximum angular velocity remains the same according to Figure 4.9.

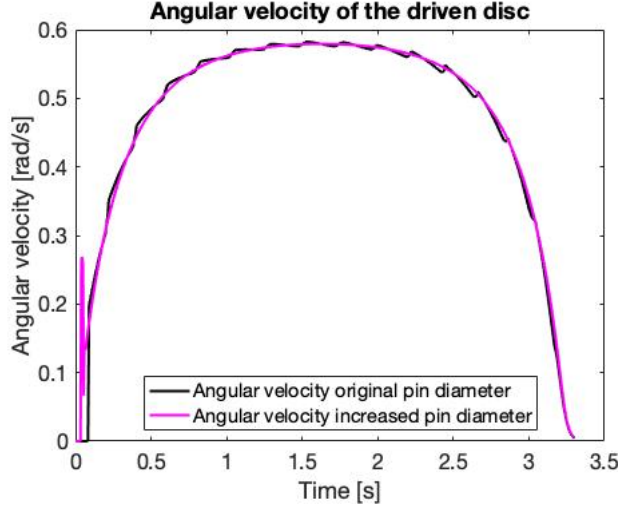


Figure 4.9: Angular velocity of the driving disc as a function of time.

The angular acceleration of the driven disc is shown in black in Figure 4.10. The various peaks in the graph occur when the pin makes sudden impacts with the slot's walls of the driven disc. Because of the size difference between pin diameter and slot width the pin bounces back and forth during the revolution. The angular acceleration of the driven disc when the pin diameter is increased to 10 mm is also shown in Figure 4.10, but in purple.

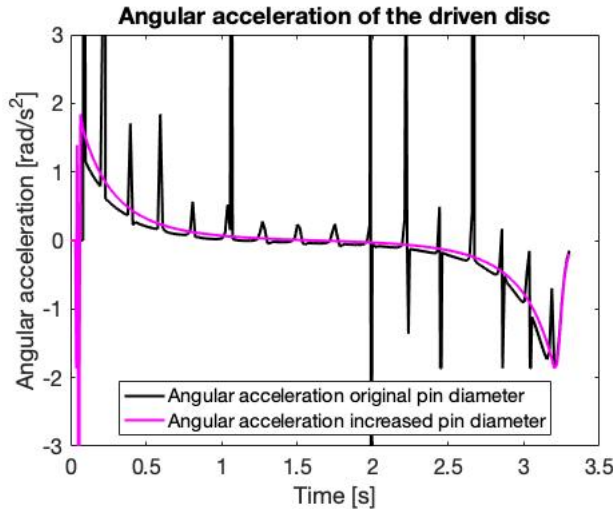


Figure 4.10: Angular acceleration of the driven disc.

5

Discussion

The last chapter in this report details the analysis of the results from the experiments and simulations presented in previous chapters. Design improvements to the internal Geneva drive is followed by a comparison of the angular velocity and angular acceleration from mathematical derivations, simulations and experiments. The details of the problems with computer vision and videos as a measuring technique as well as an analysis of the margin of error for the experiments will be stated. The last section is a summary of the project.

5.1 Design improvements

A problem with the current design that was discovered during the experiment was the over rotation of the driven disc. When the pin leaves the slot, the driven disc should come to a complete stop and therefore be perfectly aligned for the pin to enter the next slot of the driven disc. If the driven disc over rotates, the pin will bounce its way in the slot, giving unwanted impacts and vibrations. Therefore the design should have implemented some sort of mechanical stop, forcing the driven disc to stop at the desired moment.

5.2 Comparison

A comparison of the angular velocity ω_2 for the different methods are obtained in Figure 5.1. Here the two kinematic relations, the simulated angular velocity from Adams and the measured angular velocity of the model are combined in one figure, showing the angular velocity ω_2 as a function of the angle on the driving disc θ_1 . As can be seen, the simulation in Adams have given a velocity very close the the kinematic relation for the varying input velocity ω_1 . The velocity from the measurement is a bit more irregular but generally seems to follow the kinematic relation for constant ω_1 , except for two spikes at the beginning.

The measurements on the model have also been used to calculate the angular acceleration of the driven disc. A comparison of angular acceleration for the different methods are made in Figure 5.2. The two kinematic variants follow each other very closely, but both the Adams simulation and the measured angular velocity have many small variations, giving rise to the sharp spikes in angular acceleration shown in Figure 5.2. The spikes shown here below in Figure 5.2 for the Adams curve and the measurement curve, indicate the impacts when the pin hits the slot and bounces.

5. Discussion

Since the impacts are stiff, the angular acceleration changes rapidly, giving rise to these spikes. Both the measures on the physical model and the Adams simulation register the impacts very well.

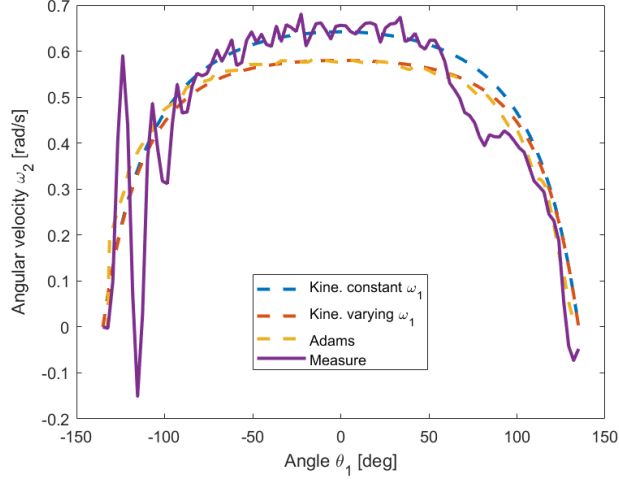


Figure 5.1: Angular velocity ω_2 of the driven disc as a function of rotation angle θ_1 for the driving disc. A comparison of the different methods.

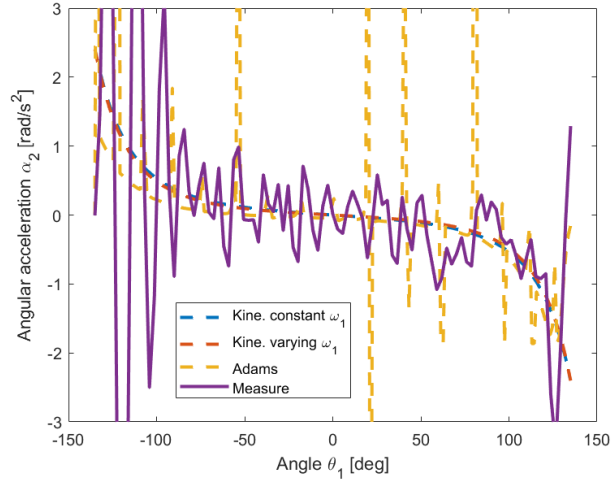


Figure 5.2: Angular acceleration α_2 of the driven disc as a function of rotation angle θ_1 for the driving disc. A comparison of the different methods.

5.3 Videos and computer vision as a measuring tool

The experimental method of using videos and computer vision to measure angles is not without problems. The first issue that was discovered is the fact that smartphone cameras do not capture videos with a constant frame rate. Figure 5.3 shows the

difference in the time between successive frames. It is clear from these plots that an assumption of constant frame rate would not be accurate, especially for the first two frames.

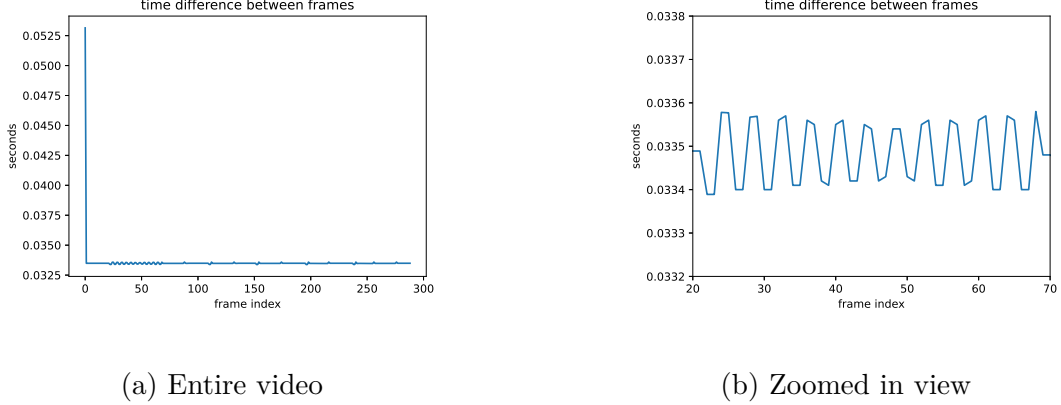


Figure 5.3: Time difference between successive frames.

Figure 5.4 shows the possible failure mode of the detection algorithm when it locates the marker's corners further into marker. It can also be noted that the center of the marker is however still well defined. This shows the importance of calculating the center point, and its angles and time derivatives.

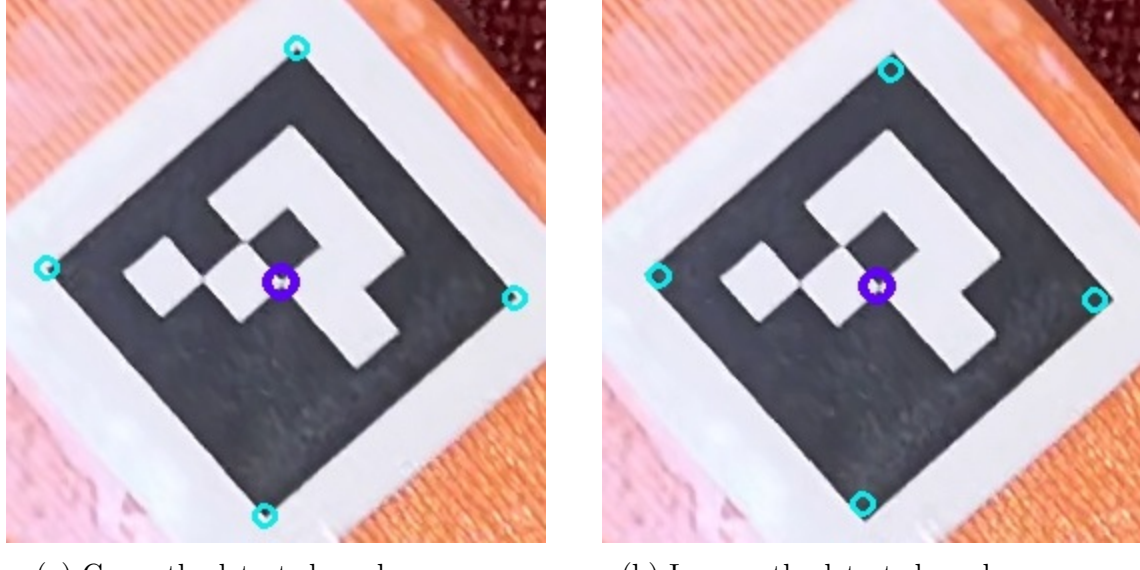


Figure 5.4: Comparison of marker detection when disc is stationary.

In section 3.2.3, it was mentioned that the experimental method was tested on both an internal- and external Geneva drive with different kinematics. The first thing that can be observed from the results is the fact that the external Geneva-drive's angular-velocity curve is much smoother during the drive sequence than the internal one, this can also be observed in the acceleration plot as a consistently negative

5. Discussion

acceleration before the local minimum and consistently positive after the local minimum.

The reason the internal Geneva drive does not exhibit the same consistency is due to the vibrations found during stationary use shown in Figure 4.5. These discontinuities are found in the external Geneva drive as well. One theory is that these small changes in where the corner is defined are not caused by vibrations but due to noise in the video causing the corners to be moved a pixel in a random direction from the real corner position. This would explain why the corners do not exhibit the same discontinuities and change independently.

This same behaviour should still be present during the rotation as well, for the internal Geneva drive this cause the change in direction for the angular velocity. The reason this does not occur in the external Geneva drive is because the angular velocity is much greater and angular acceleration is highest right before and after the local minimum. When the corner is misplaced for the Geneva drives at any point during its rotation it would either increase or decrease the velocity, the reason this will not cause a positive acceleration to become negative or vice versa is simply due to magnitude. If the acceleration is already large, small discontinuities will be less pronounced but if the acceleration is already small, the discontinuities will be very obvious. The discontinuities can still be observed in the external Geneva drive as changes in the acceleration, but they are simply not large enough to change the direction of the velocity.

The error induced by the random motion of the corner points and center point of the marker can be calculated. From Figure 4.5 it can be observed that the center point moves no more than half a pixel in x - or y -direction for a given time step. In the case of the rotation angle the worst case will equate to $1/\sqrt{2}$ pixels of perpendicular motion. The rotation angle is then given by the distance to the center of rotation which in this case was 744 pixels. The rotation caused by half a pixels movement in x - and y -direction at the right time is then 0.00095 rad or 0.05° .

If this rotation occurs during the smallest time step of 0.0333 s , the angular velocity would be 0.0285 rad/s and the angular acceleration would be 0.856 rad/s^2 . From one time step to another the angular velocity could therefore be mistakenly reduced by up to 0.0285 rad/s and in a next time step mistakenly increased by 0.0285 rad/s causing a change in angular velocity of up to 0.057 rad/s . For the angular acceleration the change could be up to 1.73 rad/s^2 . Comparing this to the observed changes for Figure 4.2 in angular velocity during the low acceleration in the middle of the drive sequence, the instantaneous changes are of a similar magnitude. For the angular acceleration from the measurements in Figure 5.2 the fluctuations are also of the same magnitude as the changes caused by the error.

The error for the corner points will be worse due to the fact that the random motion causes larger jumps and the distance to the center of rotation is shorter for some of the corners. In short, the error from the detection algorithm misplacing the

corners is minimized by placing the fiducial marker further away from the center of rotation in the image and by increasing the resolution of the image. Furthermore since the error causes an angular velocity and angular acceleration the frame rate could be reduced. The alternative to heavily decrease the frame rate and decrease the rotational velocity is probably not an option, even though the error would be minimized, since the angular velocity to measure is in turn reduced, the error will still be noticeable and the impacts would be impossible to detect.

5.4 Adams results and improvements

The reason behind the edgy appearance of the velocity graph in Figure 4.9 is the gap between the pin and the slot. The sudden increases and decreases of the angular velocity is because of the pin that bounces back and forth during the revolution. Those steep tangents of the angular velocity graph describe the angular acceleration, which is shown in Figure 4.10. Even though the velocity graph in Figure 4.9 does not look smooth, it is close to the measured angular velocity, viewed in Figure 4.2.

When the pin diameter was increased, no room for bouncing was allowed. That is why the angular velocity graph when the pin diameter is increased, shown in Figure 4.9 has a significantly smoother look than the graph with the original pin diameter. The notch in the very beginning (time < 0.1 s) of the figure is generated because of the design of the driven disc. The slot width is slightly increased towards the disc hub, which allows a bounce when the pin enters, creating the notch.

5.5 Summary

Altogether, the project has included many different engineering fields that have all been merged together to form this project. A design of an internal Geneva drive including support fixtures and motor holders have been produced using CAD software. These parts have been 3D-printed and assembled into a fully working internal Geneva drive. The design has been imported into Adams where simulations of angular velocities, accelerations and impacts have been executed. In parallel, a measuring technique have been developed for measuring movements of small fiducial markers using a smartphone camera. The measuring technique have enabled accurate measurements of the 3D-printed Geneva drive, which have been processed into angular velocities and angular accelerations of the two discs. To tie everything together, comparisons between the measurements and the simulations have been made with the theoretical kinematic behaviour of the internal Geneva drive. Impacts have been clearly detected by the measurements. The projects aim has been addressed and problem definition fulfilled with satisfactory results.

5. Discussion

Bibliography

- [1] “Geneva drive,” *Wikipedia*. Accessed March 28, 2022. [Online]. Available: https://en.wikipedia.org/wiki/Geneva_drive
- [2] Rashid, “Geneva drive – working, types and applications,” *Mechanical Walkins*, July 8, 2019, Accessed March 28, 2022. [Online]. Available: <http://www.mechanicalwalkins.com/geneva-drive-working-types-and-applications/>
- [3] Mechanical Jungle, “Working of Geneva Drive,” Accessed Apr. 26, 2022. [Online]. Available: <https://mechanicaljungle.com/working-of-geneva-drive/>
- [4] By The original uploader was Booyabazooka at English Wikipedia. - Transferred from en.wikipedia to Commons., CC BY-SA 3.0. [Online]. Available: <https://commons.wikimedia.org/w/index.php?curid=4527327>
- [5] By Coolhandscot - Own work, SolidWorks, Public Domain,. [Online]. Available: <https://commons.wikimedia.org/w/index.php?curid=1088021>
- [6] By Christophe Dang Ngoc Chan (Cdang), CC BY-SA 3.0., [Online]. Available: <https://commons.wikimedia.org/w/index.php?curid=52870145>
- [7] Wikipedia, “Image noise,” May. 3, 2022, accessed May 8, 2022. [Online]. Available: <https://en.wikipedia.org/wiki/Friction>
- [8] Erik Gustafsson, “Investigation of friction between plastic parts,” Chalmers University of technology, division of solid mechanics, Tech. Rep., 2013. [Online]. Available: <https://publications.lib.chalmers.se/records/fulltext/181751/181751.pdf>
- [9] F. Romero-Ramirez, R. Muñoz-Salinas, and R. Medina-Carnicer, “Speeded up detection of squared fiducial markers,” *Image and Vision Computing*, vol. 76, 06 2018.
- [10] S. Garrido-Jurado, R. Muñoz-Salinas, F. Madrid-Cuevas, and R. Medina-Carnicer, “Generation of fiducial marker dictionaries using mixed integer linear programming,” *Pattern Recognition*, vol. 51, 10 2015.
- [11] S. Garrido-Jurado, R. Muñoz-Salinas, F. J. Madrid-Cuevas, and M. J. Marín-Jiménez., *Aruco library documentation*, openCV version 4.5.5, June 2014. [Online]. Available: <https://docs.google.com/document/d/1QU9KoBtjSM2kF6lTOjQ76xqL7H0TEtXriJX5kwi9Kgc/edit>
- [12] Wikipedia, “Inter frame,” Jan. 21 2022, Accessed May 11, 2022. [Online]. Available: https://en.wikipedia.org/wiki/Inter_frame
- [13] ——, “Image noise,” March. 3, 2022, Accessed May 8, 2022. [Online]. Available: https://en.wikipedia.org/wiki/Image_noise
- [14] PTC, “Creo parametric,” software, version 6.0.2.0 2019. [Online]. Available: <https://www.ptc.com/en>
- [15] F. Bellard, *FFmpeg*, 5.0 Lorentz, 2022. [Online]. Available: <https://ffmpeg.org/>

Bibliography

A

Contribution report

Josef

Josef has been working a lot with the Adams model with support from Frida. Wrote the sections concerning Adams. He has been the contact person of the group, scheduling the meetings with the supervisor and making sure all parts has been ordered.

Gustav

Wrote the Pythyon script that preforms everything necessary to evaluate the experiments that were done, from FFmpeg implementation, ArUco marker detection to plotting results (<https://github.com/gurrajo/Geneva>). Wrote all sections regarding experiments and computer vision, (sections: 2.4, 3.2, 4.1, 5.3).

Frida

Frida has been working in Adams with help from Josef.
main chapters: abstract, 2.3, (1.1 1.2 with Clara)

Filip

Filip has designed and produced the CAD models that were used for 3D-printing. He has also derived the kinematics of the internal Geneva Drive. Text wise, he has written sections 2.2, 3.1, 4.2, 5.1, 5.2 and 5.5.

Clara

Clara have been responsible for 3D-printing the model, as well as helping Filip with the design of the model. Clara have also written several parts in the report, both as main writer and co-writer. The parts that Clara has been the main writer on is section 2.1. Section 1.1, 1.2, 1.2 and 3.1 has Clara been co-writer on.

Summary

It is estimated that all the group members have contributed with a similar amount of time and effort.

A. Contribution report

B

Comments on the learning process

Together, the group has learnt a lot about the process of designing and printing a model. We have experienced that communication is key to a successful work and that it is important that everybody knows what the others are working with. We have learnt to develop a 3D-prototype model in Creo parametric and how to print it in an effective way. We have learnt to make computational measurement using Adams focusing on relevant aspects. We have developed a more comprehensive understanding of how the artificial intelligence works in this case and what problems that may occur.

DEPARTMENT OF MECHANICS AND MARITIME SCIENCES

CHALMERS UNIVERSITY OF TECHNOLOGY

Gothenburg, Sweden

www.chalmers.se



CHALMERS
UNIVERSITY OF TECHNOLOGY